DIAGNOSTICS OF A CRACK IN A LOAD COUPLING OF A GAS TURBINE USING THE MACHINE MODEL AND THE ANALYSIS OF THE SHAFT VIBRATIONS

Paolo Pennacchi, Andrea Vania
Department of Mechanics
Politecnico di Milano
Via La Masa, 34, I–20156, Milan, Italy
paolo.pennacchi@polimi.it, andrea.vania@polimi.it

ABSTRACT

The diagnostics of malfunctions that can cause catastrophic failures has to be made in early stage in the industrial environment. Often flexible couplings are employed in industrial rotating machines when gearboxes and heavy thermal gradients are present. The hot and cold alignment of these couplings can be very different.
Severe misalignments can generate cracks in the stub shafts, which can propagate in operating condition. Owing to the flexural flexibility of the load coupling, the shaft vibrations may be not noticeably affected by some typical symptoms that usually point out the presence of a crack, like twice per revolution harmonics in the vibration spectrum. Anyhow, suitable diagnostic strategies can detect clear fault symptoms, while model–based methods can confirm the occurrence of the shaft bow induced by the progressive yielding of a load coupling due to a crack.
This paper shows as a model-based diagnostic methodology would have allowed a crack in a load coupling of a gas turbine to be identified before a serious failure happened by means of the shaft vibration analysis under operating conditions and rated speed.
Finally, the vibrations caused by the shaft bow due to the propagation of a crack in the stub shaft of the coupling have been simulated using suitable equivalent excitations, the magnitude and phase of which have been estimated by means of a model–based identification method.

1. INTRODUCTION

First studies on the misalignment date back to the ’60, while more recent contributions are given by [1][2][3][4][5][6] although they are generally referred to test rigs or to theoretical models. Moreover, the flexibility of the coupling is of basic importance of the dynamical behaviour caused by the misalignment. Rigid couplings are analyzed in [7][8]. An experimental study on a flexible coupling of a generator is reported in [9].
The static cold alignment of the machine–train of power units can be rather different in comparison to the hot dynamic alignment [10]. Moreover, the steady state temperature of the machine can show considerable differences along the longitudinal axis of the shaft–train. Owing to this, under the hot condition, the vertical displacements that affect the compressor end of gas–turbines are rather different from those that occur at the hot turbine end.
Therefore, the cold static alignment must compensate the different displacements that affect machine casings and pedestals along the shaft–train when the machine thermal state changes from cold to hot. However, the changes in the shaft–train alignment caused by the machine heating are not easy to be measured or predicted and the exact repeatability of these phenomena is uncertain.

Sometimes, the evaluation of the correct static alignment of large rotating machines is not a trivial task.
The alignment procedure becomes more complex when load couplings and auxiliary shafts are present in the rotor–train. Misalignments cause forces at the couplings that should not otherwise be present. These forces induce vibrations and additional alternating stresses [11] on couplings and shafts. Given high enough stresses and sufficient operating time, the endurance limit of the materials may be exceeded and the shaft or flexible units of the coupling may fail. Undesired defects in welds that may be present in the shaft [12] or in the load coupling units can generate a crack which may propagate under the effects of high dynamic stresses. Owing to the mechanical properties of the coupling units, the machine vibrations may not be affected by some typical symptoms that allow shaft cracks to be timely detected. This may cause unexpected catastrophic failures.
This paper shows the results of the analysis of the shaft vibrations of an industrial gas turbine, the load coupling of which suffered a serious failure in on–load operating conditions. The propagation of a crack in the weld area close to a diaphragm caused a local bow of the coupling stub shaft as well as changes only in the synchronous vibrations (1X). A radial misalignment of the machine–train made the crack propagation easier.
Unfortunately, in the first stage of the fault development, the 1X vibrations caused by the crack were partly compensated and masked by the vibrations induced by the shaft residual unbalance and machine misalignment. Only the final growth of the crack caused a significant rise of the 1X vibration levels, however they did not exceed the machine trip limits. The final stage of the fault development was rather fast and the load coupling unexpectedly failed causing a catastrophic damage (Figure 1). The common symptom of the presence of a crack [13], i.e. twice per revolution (2X) vibration, was practically absent during the crack growth, being masked by the high flexibility of the stub shaft.
In the paper a diagnostic strategy that would have allowed some clear fault symptoms to be timely detected, even in presence of clashing symptoms, is shown. Model–based methods aimed at the identification of faults in rotating machines have been combined with simple procedures which would have allowed the crack depth development to be pointed out. The growth of the fault severity in the time, at rated speed, has been studied and the vibrations caused by the shaft bow due to the crack propagation have been simulated using suitable bending moments the magnitude and phase of which have been estimated by means of a model–based identification method.
This case study shows how common monitoring data can be managed and analysed using on–line and off–line diagnostic strategies in order to timely detect machine faults. Moreover, this investigation shows that the crack propagation occurred in the stub shaft of the load coupling could be timely detected although the changes in the 2X vibrations were negligible.

2. EFFECT OF CRACK IN ROTATING SHAFTS

It is well-known in rotor-dynamics literature that the effect of a crack in a horizontal rotating shaft is the “breathing” of the crack (see for instance the comprehensive reviews in [14][15][16] and [17] for the breathing mechanism). This corresponds to a periodical variation of the shaft stiffness, which is local in the neighbourhood of the crack in rotors of real machines. The breathing mechanism is commonly taken into account by using some sort of lumped and

localized variable stiffness in correspondence of the crack. This is possible if both a continuous approach, see i.e. [18], or a finite element modelling is used. In the last case, crack modelling is rather straightforward: the stiffness matrix $[\mathbf{K}(\Omega t)]_j$ of the cracked element j (Figure 2) is periodical due to the breathing of the crack and can be expanded in a Fourier's series:

$$\left[\mathbf{K}(\Omega t)\right]_j = \left[\mathbf{K}_m\right]_j + \sum_k \left[\Delta\mathbf{K}_k\right]_j \mathrm{e}^{\mathrm{i}k\Omega t} \tag{1}$$

where Ω is the rotating speed.

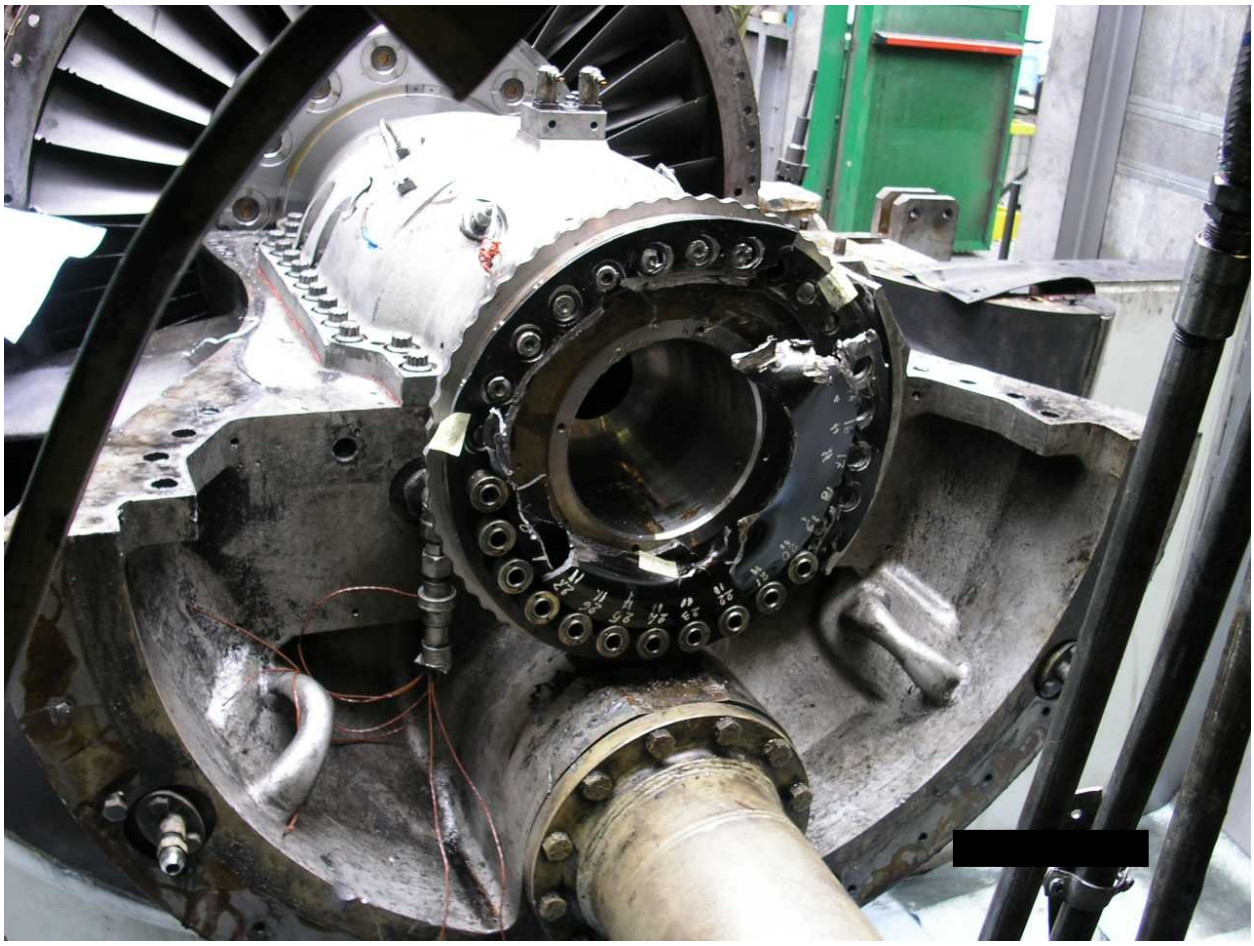

Figure 1. Load coupling after failure.

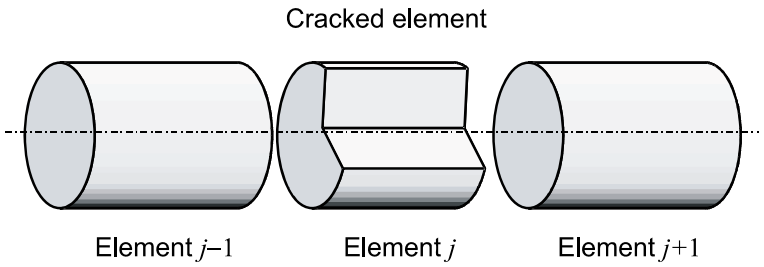

Figure 2: Cracked element in a finite element model of a shaft.

When the complete rotor system is considered, the presence of the periodic term in eq. (1) causes the periodicity of the system stiffness matrix. If the Fourier's expansion is now truncated in correspondence of the third harmonic component for simplicity, it results:

$$\left[\mathbf{K}\left(\Omega t\right)\right]=\left[\mathbf{K}_m\right]+\left[\Delta\mathbf{K}_1\right]\mathrm{e}^{\mathrm{i}\Omega t}+\left[\Delta\mathbf{K}_2\right]\mathrm{e}^{\mathrm{i}2\Omega t}+\left[\Delta\mathbf{K}_3\right]\mathrm{e}^{\mathrm{i}3\Omega t} \tag{2}$$

Matrices $\left[\Delta\mathbf{K}_n\right]$ are sparse, because their elements are different from 0 only in the positions corresponding to the cracked element nodes. The equations of motions of the rotor system are:

$$\left[\mathbf{M}\right]\ddot{\mathbf{x}}_t+\left[\mathbf{C}\right]\dot{\mathbf{x}}_t+\left[\mathbf{K}(\Omega t)\right]\mathbf{x}_t=\mathbf{F}_e+\mathbf{W} \tag{3}$$

where Ω is the rotating speed, $\left[\mathbf{M}\right]$ is the mass matrix, $\left[\mathbf{C}\right]$ the damping matrix (including gyroscopic effects), $\mathbf{F}_e$ the external rotating forces (unbalance, bow, etc.) and $\mathbf{W}$ is the statical force vector (weight and so on). By substituting the stiffness expansion eq. (2) in eq. (3), the following equation is obtained:

$$\left[\mathbf{M}\right]\ddot{\mathbf{x}}_t+\left[\mathbf{C}\right]\dot{\mathbf{x}}_t+\left(\left[\mathbf{K}_m\right]+\sum_{j=1}^{3}\left[\Delta\mathbf{K}_j\right]\mathrm{e}^{\mathrm{ij}\Omega t}\right)\mathbf{x}_t=\mathbf{F}_e+\mathbf{W} \tag{4}$$

The generalized displacement $\mathbf{x}_t$ can be split in its statical $\mathbf{x}_s$ and dynamical $\mathbf{x}$ components:

$$\mathbf{x}_t=\mathbf{x}_s+\mathbf{x} \tag{5}$$

where the statical component is given by:

$$\mathbf{x}_s=\left[\mathbf{K}_m\right]^{-1}\mathbf{W} \tag{6}$$

According to eq.(5), eq.(7) is finally obtained.

$$\left[\mathbf{M}\right]\ddot{\mathbf{x}}+\left[\mathbf{C}\right]\dot{\mathbf{x}}+\left[\mathbf{K}_m\right]\mathbf{x}=\mathbf{F}_e-\sum_{j=1}^{3}\left[\Delta\mathbf{K}_j\right]\mathrm{e}^{\mathrm{ij}\Omega t}\left(\mathbf{x}_s+\mathbf{x}\right) \tag{7}$$

Since for linear systems the vibration $\mathbf{x}$ component is periodical, it can be expanded in Fourier's series too. If its *n*-th harmonic component is taken into account, it can be expressed as the sum of two counter rotating vectors:

$$\mathrm{Re}\left(\mathbf{x}_n\,\mathrm{e}^{\mathrm{i}n\Omega t}\right)=\frac{1}{2}\mathbf{x}_n\,\mathrm{e}^{\mathrm{i}n\Omega t}+\frac{1}{2}\mathbf{x}_n^{*}\,\mathrm{e}^{-\mathrm{i}n\Omega t} \tag{8}$$

Similarly, the *n*-th component of Fourier's expansion of the periodical stiffness $\left[\Delta\mathbf{K}_n\right]$ can be written as:

$$\mathrm{Re}\left(\left[\Delta\mathbf{K}_n\right]\mathrm{e}^{\mathrm{i}n\Omega t}\right)=\frac{1}{2}\left[\Delta\mathbf{K}_n\right]\mathrm{e}^{\mathrm{i}n\Omega t}+\frac{1}{2}\left[\Delta\mathbf{K}_n^{*}\right]\mathrm{e}^{-\mathrm{i}n\Omega t} \tag{9}$$

Accordingly to the previous assumption, the Fourier's expansion of both eqs. (8) and (9) is limited to the third harmonic component. If the product in the last term of eq. (7) is calculated using eqs. (8) and (9), the result has harmonics up to sixth order. Anyway if only the components up to the the third harmonic component are taken into account and higher order components are disregarded, then the following equivalent exciting component vectors can be defined:

$$\widehat{\mathbf{F}}_{f_0} = -\left(\frac{1}{4}\left[\Delta\mathbf{K}_1\right]\mathbf{x}_1^* + \frac{1}{4}\left[\Delta\mathbf{K}_1^*\right]\mathbf{x}_1 + \frac{1}{4}\left[\Delta\mathbf{K}_2\right]\mathbf{x}_2^* + \frac{1}{4}\left[\Delta\mathbf{K}_2^*\right]\mathbf{x}_2 + \frac{1}{4}\left[\Delta\mathbf{K}_3\right]\mathbf{x}_3^* + \frac{1}{4}\left[\Delta\mathbf{K}_3^*\right]\mathbf{x}_3 \right) \tag{10}$$

$$\widehat{\mathbf{F}}_{f_1} \mathrm{e}^{\mathrm{i}\Omega t} = -\left(\left[\Delta\mathbf{K}_1\right]\mathbf{x}_s + \frac{1}{2}\left[\Delta\mathbf{K}_2\right]\mathbf{x}_1^* + \frac{1}{2}\left[\Delta\mathbf{K}_3\right]\mathbf{x}_2^* + \frac{1}{2}\left[\Delta\mathbf{K}_1^*\right]\mathbf{x}_2 + \frac{1}{2}\left[\Delta\mathbf{K}_2^*\right]\mathbf{x}_3 \right) \mathrm{e}^{\mathrm{i}\Omega t} \tag{11}$$

$$\widehat{\mathbf{F}}_{f_2} \mathrm{e}^{\mathrm{i}2\Omega t} = -\left(\left[\Delta\mathbf{K}_2\right]\mathbf{x}_s + \frac{1}{2}\left[\Delta\mathbf{K}_3\right]\mathbf{x}_1^* + \frac{1}{2}\left[\Delta\mathbf{K}_1\right]\mathbf{x}_1 + \frac{1}{2}\left[\Delta\mathbf{K}_1^*\right]\mathbf{x}_3 \right) \mathrm{e}^{\mathrm{i}2\Omega t} \tag{12}$$

$$\widehat{\mathbf{F}}_{f_3} \mathrm{e}^{\mathrm{i}3\Omega t} = -\left(\left[\Delta\mathbf{K}_3\right]\mathbf{x}_s + \frac{1}{2}\left[\Delta\mathbf{K}_1\right]\mathbf{x}_2 + \frac{1}{2}\left[\Delta\mathbf{K}_2\right]\mathbf{x}_1 \right) \mathrm{e}^{\mathrm{i}3\Omega t} \tag{13}$$

Eqs. (11), (12) and (13) are respectively the first, the second and the third harmonic components of the crack equivalent excitation acting on the system. Obviously, if higher order expansions are considered in the previous equations, then also the crack excitation will contain these harmonic components. Since these excitations are 1X, 2X and 3X (and higher…) of the rotating speed, also the vibrations caused by the crack have 1X, 2X and 3X (and higher…) components.

This explains why in a machine equipped by a suitable condition monitoring system, a change in 1X, 2X and 3X vibration vector is considered as a crack symptom. A change in vibration vector means not just an increase or a decrease in amplitude, but also a change in phase only with constant amplitude. However, 1X components could be caused by many other faults (e.g. unbalance, bow, coupling misalignments) and 2X components can be due also to polar stiffness asymmetries (in generators), to surface geometry errors (journal ovalization) and to non-linear effects in oil film bearings. These two last causes can also generate 3X components, which are generally very small.

Since faults generating 1X components are more common than those of 2X, the symptom of cracked shaft normally indicated in literature is related to 2X. Anyhow, it is important to note that, if the 1X crack excitation is not masked by other faults with 1X components, the 1X vibration change is a crack symptom in every respect.

Moreover, note that the projections along reference axes of the harmonic component of the excitation system in Eqs. (11), (12) and (13) are not necessarily equal, thus the excitation system is not in general represented by rotating forces or moments. Actually, in [19] it is shown that the bending moments due to the crack are prevalent in the equivalent excitation system, which can be written in a general form as:

$$\mathbf{F}_{f_n}^{(x,y)} = \left\{ \mathbf{F}_L^{(x,y)} \right\} \overline{A}^{(x,y)} \tag{14}$$

where $\left\{ \mathbf{F}_L^{(x,y)} \right\}$ is the localisation vector, which has all null-elements except for the degrees of freedom (d.o.f.) to which the exciting system is applied, and $\overline{A}^{(x,y)}$ is a complex number representing the amplitudes $M_n^{(x)}, M_n^{(y)}$ and the phases $\varphi_n^{(x)}, \varphi_n^{(y)}$ of the excitation (Figure 3).

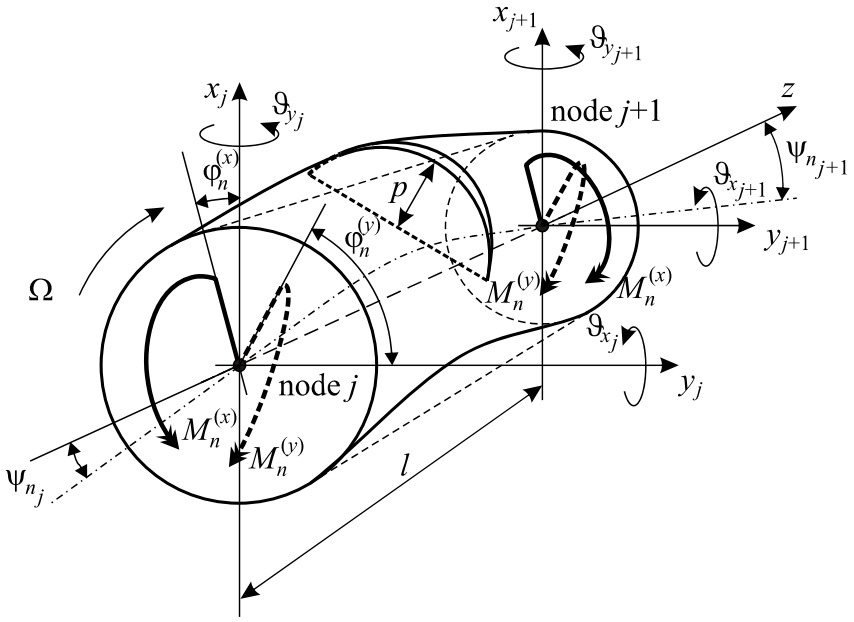

Figure 3: Equivalent bending moments acting on the cracked element.

In extended form, by considering a finite element model composed by beam elements with 4 d.o.f.s per node ordered as $\{x \;\; \vartheta_x \;\; y \;\; \vartheta_y\}$, for a crack located in the j-th element of the shaft line, the corresponding equivalent force systems are:

$$\begin{aligned}
\mathbf{F}_{f_n}^{(x)} &= \Big\{ 0 \;\vdots\; \underbrace{0 \;\; i \;\; 0 \;\; 0}_{j\text{-th rotor node}} \;\; \underbrace{0 \;\; -i \;\; 0 \;\; 0}_{j+1\text{-th rotor node}} \;\vdots\; 0 \;\; \underbrace{0 \;\cdots\; 0}_{\text{foundation d.o.f.s}} \Big\}^{\mathrm{T}} \cdot M_n^{(x)} \mathrm{e}^{\mathrm{i}\varphi_n^{(x)}} = \\
&= \left\{ \mathbf{F}_{L_j}^{(x)} \right\} \bar{A}_n^{(x)}, \quad n = 1,2,3 \\
\mathbf{F}_{f_n}^{(y)} &= \Big\{ 0 \;\vdots\; \underbrace{0 \;\; 0 \;\; 0 \;\; 1}_{j\text{-th rotor node}} \;\; \underbrace{0 \;\; 0 \;\; 0 \;\; -1}_{j+1\text{-th rotor node}} \;\vdots\; 0 \;\; \underbrace{0 \;\cdots\; 0}_{\text{foundation d.o.f.s}} \Big\}^{\mathrm{T}} \cdot M_n^{(y)} \mathrm{e}^{\mathrm{i}\varphi_n^{(y)}} = \\
&= \left\{ \mathbf{F}_{L_j}^{(y)} \right\} \bar{A}_n^{(y)}, \quad n = 1,2,3
\end{aligned} \tag{15}$$

where the only terms different from zero are those relative respectively to the rotational horizontal and vertical d.o.f.s of the extreme nodes of cracked element j. The model based identification procedure for the crack is reported in detail in appendix.

3. CASE HISTORY

The shaft vibrations of a 100 MW power unit have been analysed. The machine–train was composed of a gas turbine, a generator and a steam turbine. Figure 4 shows the machine–train layout. In the same figure the numbers of the journal bearings used in the paper are shown. Each bearing was equipped with two proximity probes mounted 90° apart (45° Left and 45° Right). A speed–reducing gearbox was installed between gas turbine and generator. Gas turbine and load

gear shaft were connected by means of a diaphragm coupling (Figure 5). The operating speeds of gas turbine and generator were 5237 rpm and 3000 rpm, respectively.

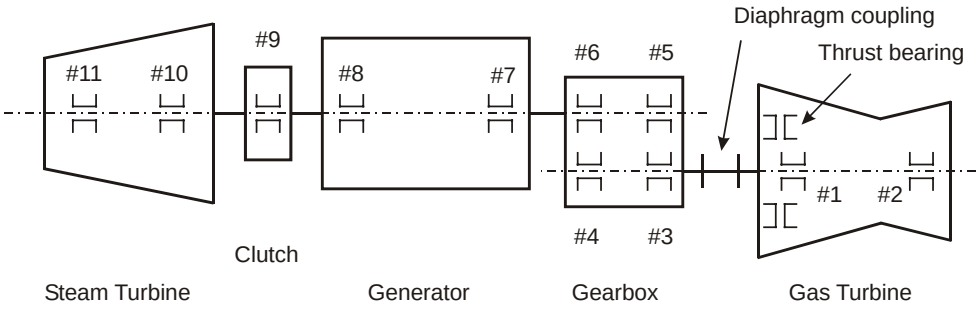

Figure 4: Machine–train layout and bearing numbers.

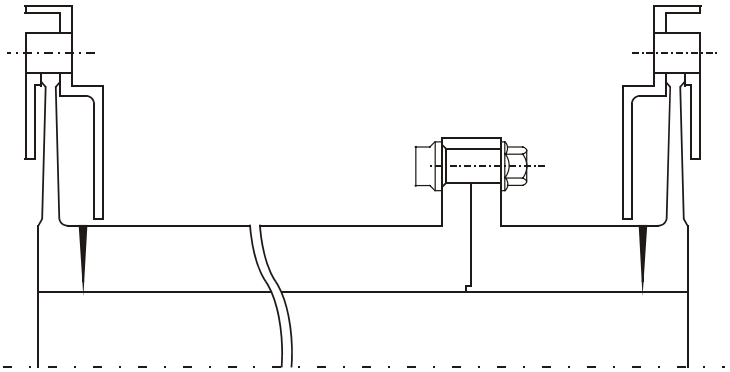

Figure 5: Diaphragm coupling.

Some important maintenance actions were carried out on the power unit during a long scheduled outage. Owing to this the machine–train was subjected to important overhauls. At the end of the maintenance the shafts of the machine–train were aligned. It was well known that the machine heating caused significant changes in the shaft–train alignment, especially in the area near the gas turbine. Therefore, the hot operating alignment showed some important differences in comparison to the static cold alignment. In this case, under hot conditions the compressor end of the gas turbine grew more in the vertical direction than the hot turbine end. These vertical displacements had to be compensated by assigning a suitable static misalignment. Therefore, the alignment between the turbine forward stub shaft and the load gear pinion flange had to be checked. In the vertical diametrical plane the flange faces should be open at the top while in the horizontal diametrical plane they should be parallel from side to side. Static cold misalignment reference values and tolerances were specified by the machine manufacturer (Figure 6).

The readings provided by a laser alignment unit showed that both parallel offset and angular misalignment exceeded the respective tolerances at the coupling between the turbine forward stub shaft and the load gear pinion flange. In order to obtain the desired alignment the gas turbine case had to be moved in the horizontal plane at both ends.

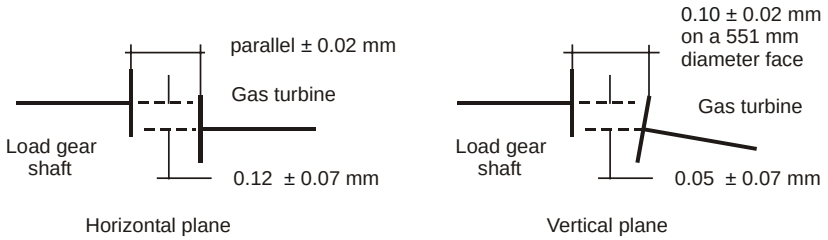

Figure 6: Parallel offset and angular misalignment tolerances.

Unfortunately, these horizontal displacements required a fixed constraint of the turbine case, located near the thrust bearing, to be unlocked. This maintenance action was not trivial. It would have required the machine outage to be extended for some further days. Owing to this, the plant personnel decided to do only some minor corrective actions the main goal of which was to reduce the angular misalignment in the vertical and horizontal planes. However, at the end of these actions the alignment between gas turbine and load gear was not yet correct. In particular, in the diametrical horizontal plane the parallel offset was rather large: 0.6 mm (Figure 8). Conversely, the flanges were parallel.

Some alignment data exceeded the tolerance values indicated by the turbine manufacturer. Anyhow they were significantly lower than the rated misalignment capacity certified by the coupling manufacturer. Therefore, this misalignment condition was supposed to be not dangerous either during run-ups and coast-downs nor in operating conditions.

This fact was also ascertain *a posteriori* by our FEM calculations based on the comparison between the technical data provided by the manufacturer of the load coupling and the values of the radial and angular misalignment measured at the end of the machine reassembling. The results of a stress analysis performed after the failure by means of a FEM of the coupling confirmed that the maximum stress induced by the misalignment was not critical for an unbroken coupling (that is in absence of cracks in the weld area), see Figure 7.

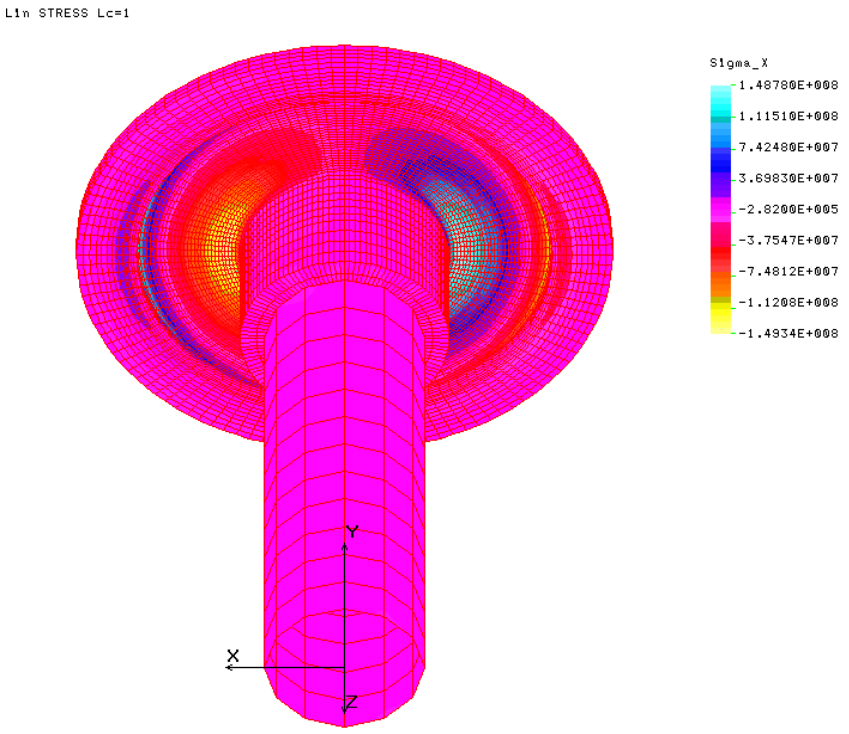

Figure 7: Stress analysis of the coupling in the operating conditions.

The real cause of the coupling failure was not the machine misalignment, that in any case was to be eliminated, but the presence of unidentified cracks in the weld area of a diaphragm of the coupling.
However, the undesired parallel offset between the axes of gas turbine and load gear shaft caused a static deflection of the machine train which affected the horizontal loads acting on the journal bearings. Likely, this caused abnormal stresses in the shafts and influenced the machine dynamic behaviour.

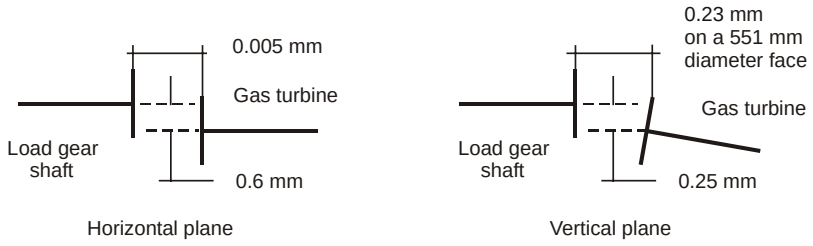

Figure 8: Final static cold alignment.

Table 1 shows the bearing loads evaluated by assigning the static alignment to a finite element model (FEM) of the shaft–train composed of load gear shaft and gas turbine (Figure 9).
The machine was started up and returned on service. The gas turbine vibrations measured in full–load operating condition were normal. The maximum level of the 1X vibrations reached 48 μm pp at bearing #1, that is at the coupling end. The 1X vibrations of the load gear shaft was very low: the maximum amplitude reached 13 μm pp. However, only three days after the return on service of the unit the level of the 1X vibrations of gas turbine and load gear shaft showed a sudden significant increase.

Table 1: Bearing loads caused by the abnormal static alignment of the shaft train composed of gas turbine and load gear shaft: data provided by the simulating model.

	BEARING N.			
BEARING LOAD	#1	#2	#3	#4
Vertical load [N]	83278	84247	15610	7859
Horizontal load [N]	1647	- 372	- 2496	1220

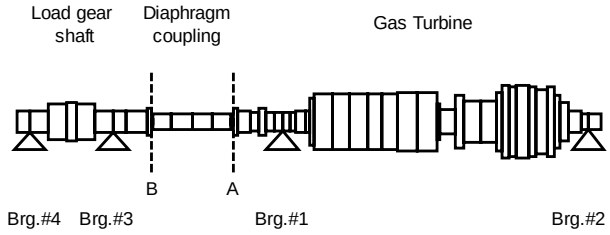

Figure 9: Finite Element Model of the fast shaft–train of the power unit (gas turbine and load gear shaft).

Hereinafter this occurrence will be denoted "fault event n.1". At the same time, also the phase of the 1X vibrations showed a quite evident instantaneous turn. Figure 10 to Figure 12 show the historical trend of the 1X vibrations measured at the two journal bearings of the gas turbine (#1, #2) as well as at the bearing #3, mounted on the load gear shaft just beyond the diaphragm coupling. Fault event n.1 corresponds to label ①. The twice per revolution (2X) vibrations measured at all the supports #1–#4 were lower than 6 μm pp (Figure 14 and Figure 15). They showed only very small changes that were ascribed to non-linear effects in the fluid-film journal bearings, induced by the significant changes in the 1X vibration vectors. The small weight of the stub-shaft of the load coupling, along with the diaphragm flexibility, limited the magnitude of the crack breathing and the levels of the 2X vibrations. The sudden increase of the 1X vibrations was a clear symptom of a fault occurrence.

Few minutes after their instantaneous abnormal growth the 1X vibration levels at bearings #1 and #2 started to decrease. This trend was slow but continuous. Also the phase of the 1X vibration vectors showed a continuous turn. Twenty hours after this abnormal event (label ②)the gas turbine vibrations were very similar to those measured just before the event occurrence (Figure 10 and Figure 11). At first, this was considered a reassuring behaviour although at bearing #3 the 1X vectors were still quite different from those evaluated before the fault (Figure 12). Anyhow their amplitude was not excessively high (55 μm pp). During the next nineteen hours the amplitude of the 1X vibrations at bearing #1 showed a progressive growth while the 1X phase at bearings #1 and #3 slowly turned.

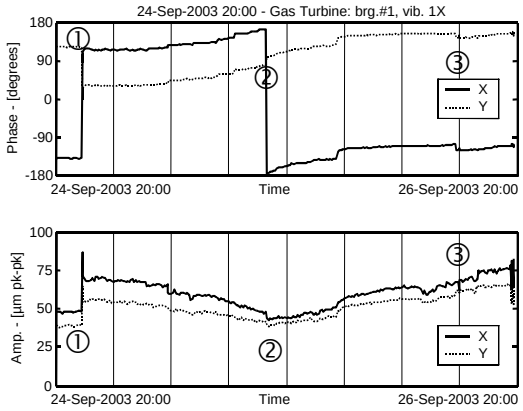

Figure 10: Historic trend of the 1X vibrations measured at bearing #1 of the gas turbine during the development of the flexible coupling failure.

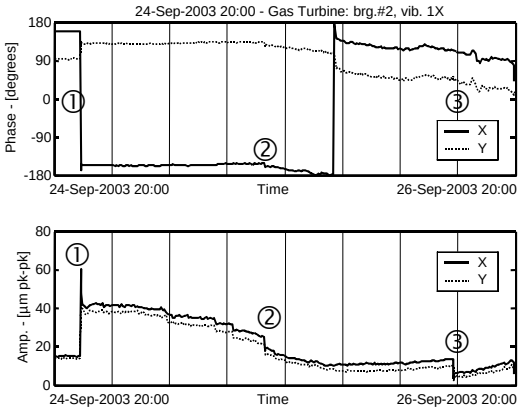

Figure 11: Historic trend of the 1X vibrations measured at bearing #2 of the gas turbine during the development of the flexible coupling failure.

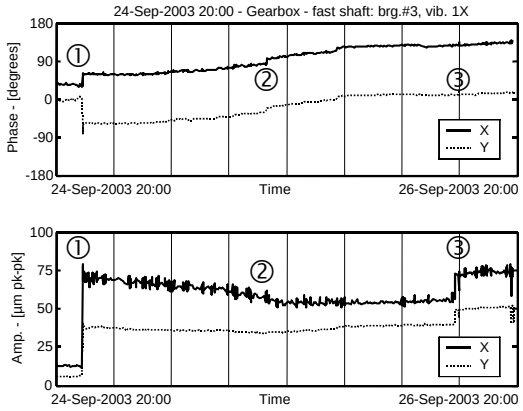

Figure 12: Historic trend of the 1X vibrations measured at brg.#3 of the fast shaft of the gearbox during the development of the flexible coupling failure.

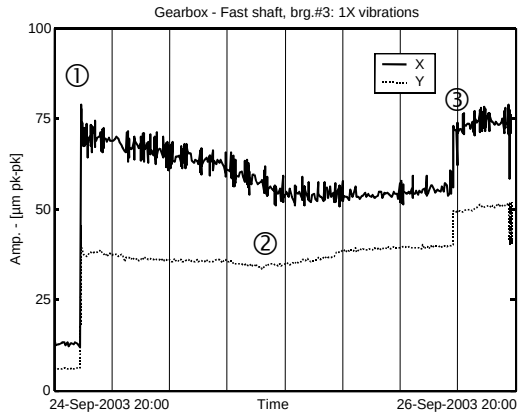

Figure 13: Historic trend of the amplitude of the 1X vibrations measured at brg.#3 of the gear shaft during the development of the flexible coupling failure.

Then, at bearing #3 the 1X vibration levels showed a further sudden growth from 58 µm pp to 73 µm pp (Figure 12). Hereinafter this occurrence will be denoted "fault event n.2" and indicated by label ③.

In the end, during the next eight hours the 1X vibrations at bearing #1 increased and reached 80 µm pp. Then, after a further fast growth of these vibration levels a catastrophic failure occurred on the diaphragm coupling. The tube yielded and the connection between gas turbine and load gear shaft failed. This primary fault induced secondary catastrophic damages on the gas turbine.

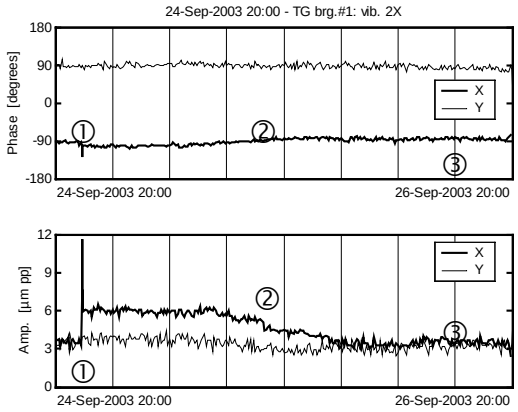

Figure 14: Historic trend of the 2X vibrations measured at bearing #1 of the gas turbine during the development of the flexible coupling failure.

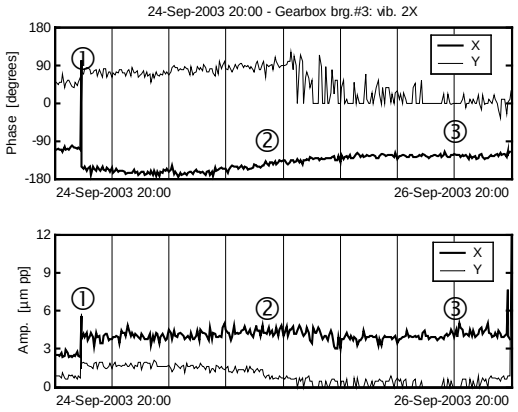

Figure 15: Historic trend of the 2X vibrations measured at brg.#3 of the fast shaft of the gearbox during the development of the flexible coupling failure.

A first visual inspection of the broken parts of the coupling showed that a deep crack propagated in the stub shaft near the coupling flange located towards the gas turbine. A further important fracture occurred in the weld area near the coupling flange towards the load gear shaft. The inspection of the broken parts and the analysis of the vibration trends indicated that the primary yielding occurred at the coupling end towards the gas turbine. This first major damage caused further subsequent damages.

Four years before, during a previous maintenance of the power unit the diaphragm coupling was inspected to verify its integrity. The two ending parts of the coupling near the flanges are welded to the stub shaft. The inspections found no failure indications in the weld area, however, near the weld area some small cracks were detected. These superficial cracks were eliminated by machining the tube surface. Therefore, it is possible to suppose that some new cracks could have grown during the next four years after this maintenance action. In addition to this, some further undetected cracks could be present from a long time, in the weld area, under the coupling tube surface. It is possible to suppose that the additional fatigue stresses induced by the machine misalignment caused the propagation of a pre–existent crack. Therefore, the torque due to the electrical load along with static and dynamic flexural loads could have caused the coupling yielding and the subsequent catastrophic fault.

The crack propagation caused a local bow of the coupling stub shaft: this induced significant changes in the 1X vibrations of gas turbine and load gear shaft. On the contrary, the presence of the diaphragms, which are very flexible, limited the growth of the 2X vibrations of the machine train. The development of the shaft bow depended on the evolution of the crack propagation. Moreover it is necessary to consider that the crack was not an *ideal* transverse crack. Owing to this it seems likely that partial *instantaneous* propagations of the crack caused small sharp changes of amplitude and phase of the 1X vibrations that are superimposed to more considerable progressive changes of the same parameters due to the continuous propagation of the crack.

The spikiness of the amplitude curve of the 1X vibrations measured in the X direction at bearing #3, mounted on the load gear shaft of the gas turbine, can be considered a further indication of the crack propagation (Figure 12 and Figure 13).

The 1X vibration vectors induced by the progressive yielding of the coupling were added to the original 1X vibrations caused by the residual imbalance and the shaft train misalignment. This, in part, masked the severity of the impending fault. In fact, after the first sudden growth, the 1X

vibration levels continuously decreased during a time interval of twenty hours. This was considered a reassuring behaviour. However, only the 1X additional vibrations actually induced by the crack should be analysed to identify the fault type and its severity. These vibration vectors can be evaluated by subtracting suitable reference vectors from the 1X vibration data collected during the fault evolution. If the non–linear effects are negligible the 1X vectors obtained with this procedure can be considered a good estimation of the 1X vibrations caused only by the shaft bow induced by the crack propagation. In the following investigations the 1X vectors measured just after the occurrence of the "fault event n.1" have been used as reference vectors.

A first qualitative study of the additional vibrations can be carried out by analysing the polar plot of the 1X vectors associated with a measurement point. Figure 16 shows the polar plot of a subset of the 1X vibrations measured at bearing #3 during the fault evolution. The origin of the 1X vectors coincides with the origin of the polar axes. The large changes in phase and magnitude of the raw vibration vectors are evident. The 1X additional vibrations can be obtained by connecting the end of the reference vector with the end of each of the further vibration vectors that are shown in the polar plot.

The bold line that connects the ends of the 1X vectors (Figure 16) generates a curve which provide some interesting information about the trend of the additional vibration vectors. In fact, on this measurement point, the magnitude of these vectors continuously grew while the phase was nearly constant. This means that the 1X equivalent excitations due to the coupling failure could be simulated by means of bending moments, that is by means of vectors whose resultant had a nearly constant phase while its magnitude increased during the failure development (see Figure 21).

These diagnostic information are quite different from those provided by the analysis of the raw vibrations. Similar results were obtained by the analysis of the data collected at all the measurement points located on gas turbine and load gear shaft.

Figure 17 shows the historical trend of magnitude and phase of the additional 1X vibrations evaluated at bearings #1 and #3 along the X and Y directions. These two bearings were located on gas turbine and load gear shaft just beyond the flanges of the diaphragm coupling. Therefore, on these cross–sections the effects of the coupling failure were more evident. The amplitude curves illustrated in Figure 17 show that the magnitude of the additional vibrations significantly increased with time while the vibration phase was nearly constant. This indicates that the crack propagation caused a local bow of the stub shaft whose severity grew with time. Although the shape of the fracture surface of the broken coupling was rather complex it is possible to suppose that this shaft bow occurred in a nearly fixed plane.

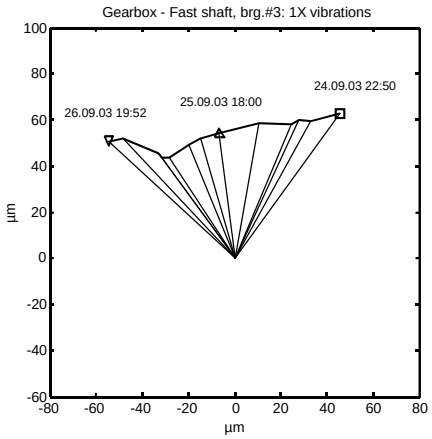

Figure 16: Polar plot of the 1X vibrations measured by the probe X mounted at bearing #3 of the gear shaft during the development of the flexible coupling failure.

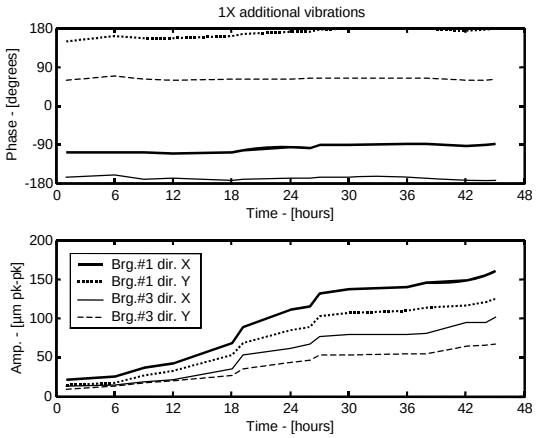

Figure 17: Historic trend of the 1X experimental additional vibrations, evaluated at brg.#1 and #3, caused by the development of the flexible coupling failure.

3.1 Identification of the crack in the diaphragm coupling

As above mentioned the machine faults and malfunctions can be modelled by means of suitable sets of equivalent excitations that are applied to some degrees of freedom of suitable nodes of the FEM of the shaft–train.

In the present case study the breathing mechanism of the crack induced a shaft local bow whose magnitude changed over a complete rotation of the shaft depending on the angular position of the crack. This phenomenon was simulated by applying pairs of opposite harmonic bending moments (1X) to the FEM of the shafts in suitable locations. These equivalent excitations were applied both in vertical and horizontal diametrical planes.

In this case study the uncertainty about the location of the equivalent excitations was limited to one of the two weld areas close to both ends of the coupling. The crack propagation caused the equivalent bending moments to be time dependent. This required several identifications of the equivalent excitations each one carried out by considering different sub–set of the vibration data collected during the fault development. The experimental evidences showed that in this case study it was unimportant to consider the 2X harmonic components, as well as higher harmonic orders, of the equivalent excitations.

Before doing the model–based identification of fault a preliminary analysis of the 1X filtered orbits described by the journals was carried out. Figure 18 shows the 1X filtered orbits measured at bearing #3, before the occurrence of the "fault event n.1", in operating conditions associated with different electrical loads. These orbits show a high ellipticity and an abnormal inclination angle of the major axis. These are symptoms of the presence of a significant horizontal pre–load which only in part is in accordance with the presence of an horizontal component of the gear load. On the contrary, it was well known that the horizontal parallel offset between the axes of gas turbine and load gear shaft caused an additional horizontal load on bearing #3 (Table 1).

Figure 19 shows some 1X filtered orbits measured at bearing #3 in operating conditions during the failure development. These orbits have been evaluated considering raw vibration data. The orbit wideness and the position of the keyphasor dot changed in the time accordingly with an ambiguous law. By comparing the orbits illustrated in Figure 18 and Figure 19 it is possible to

note that the first significant propagation of the crack caused important changes in the orbit shape. This is a consequence of the higher flexibility of the coupling tube induced by the crack development.

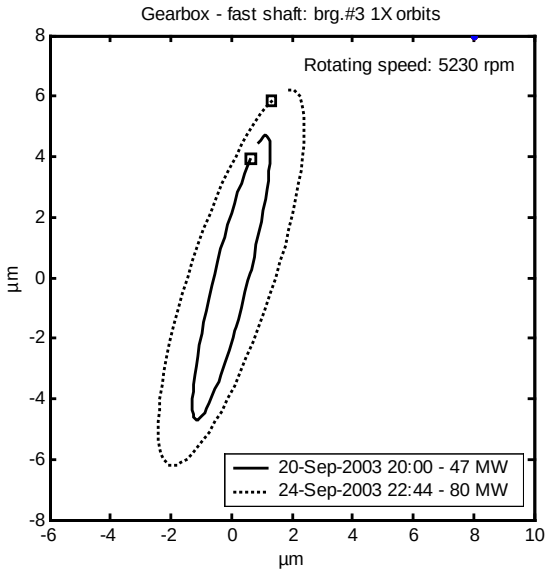

Figure 18: Gearbox, fast shaft, bearing #3: 1X filtered orbits measured in operating conditions associated with different electrical loads, before the failure occurrence.

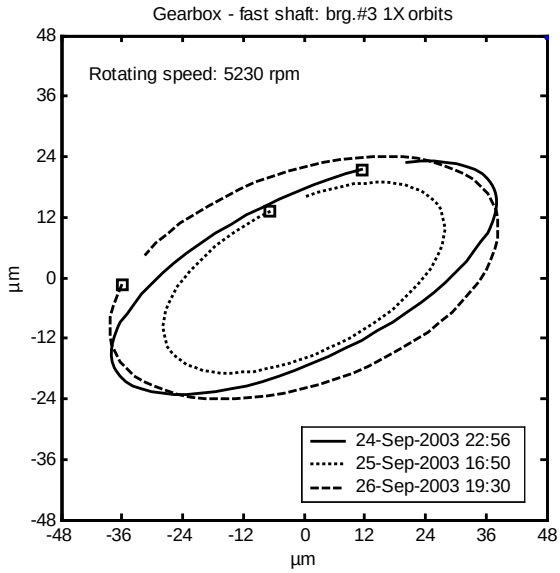

Figure 19: Gearbox, fast shaft, bearing #3: 1X filtered orbits measured in operating conditions during the failure development.

In the end, the additional 1X vibrations associated with the raw vibrations used to evaluate the orbits illustrated in Figure 19 have been considered. Figure 20 shows the 1X filtered orbits obtained on the basis of these additional vibrations. In this case the orbit wideness increased continuously during the failure development while the keyphasor dot remained in a fixed position along the orbits. Also the inclination angle of the major axis of these orbits remained constant during the fault development. These results are in accordance with the assumption that the magnitude of the bending moments due the shaft bow increased continuously during the crack propagation as well as with the assumption that the resultant of the 1X equivalent bending moments lays in a fixed plane.

Figure 9 shows also the two cross–sections (A, B) of the gas turbine located near the weld areas where the equivalent excitations have been applied. A first identification process of the fault was carried out by considering two pairs of opposite bending moments applied in the horizontal and vertical diametrical planes in the cross–section A, that is near the coupling flange towards the gas turbine (Figure 9). The equivalent excitations were identified considering the additional 1X vibrations of gas turbine and load gear shaft evaluated accordingly with the procedure above described. Magnitude and phase of the two pairs of opposite the bending moments were estimated for different stages of the fault development.

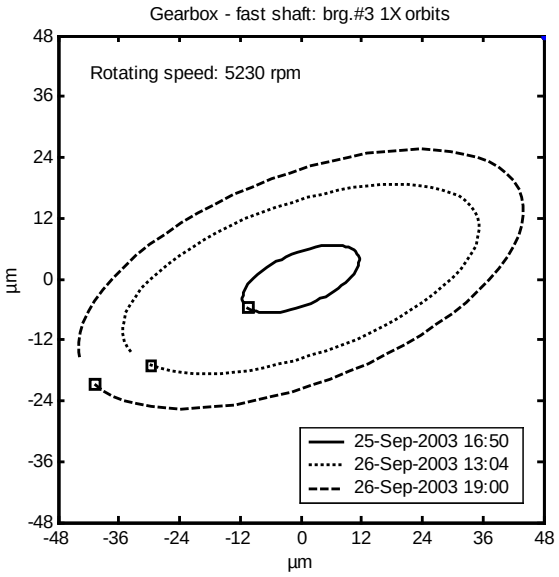

Figure 20: Gearbox, fast shaft, bearing #3: 1X filtered orbits evaluated in operating conditions during the failure development. Orbits obtained considering the additional vibrations caused by the coupling failure.

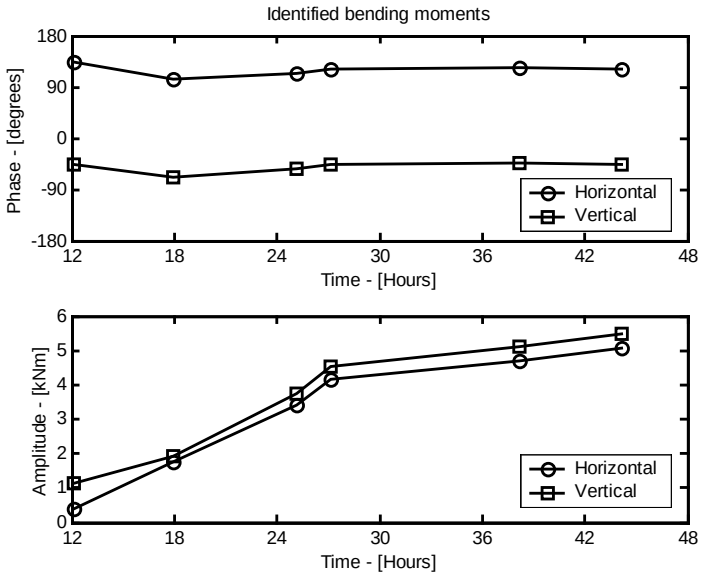

Figure 21: Identified bending moments: trend curves of amplitude and phase of the equivalent moments applied in the horizontal and vertical diametrical planes.

Figure 21 shows the amplitude and phase curves of the identified bending moments. In this figure the phase of only one moment of each pair of opposite bending moments is shown. It is possible to note that the magnitude of the moments applied in the horizontal and vertical diametrical planes continuously increases with the time while the phase is nearly constant. These results are in accordance with the trend of the experimental additional vibrations induced by the crack propagation (Figure 17). Each case study that has been considered during the fault evolution the model–based identification method provided the evaluation of a residual, ε. The mean value and the standard deviation of these residuals were 0.3816 and 0.0231 respectively. These results indicate that for each case study the identification error was rather small.

As said above the shaft vibrations were mainly synchronous with the rotating speed. The elliptical orbits defined considering the 1X additional vibrations depend on amplitude and phase of the vibrations evaluated in the two orthogonal directions X and Y. Therefore, significant indications about the accuracy of the identification process can be obtained by comparing the experimental orbits with those defined on the basis of the numerical results provided by the simulating model. The amplitude of the major and minor axes of the orbit are the parameters that have been considered to analyse the wideness and the shape of the 1X elliptical orbits.

Figure 22 and Figure 23 show the comparison between experimental and theoretical amplitudes of the major and minor axes of the orbits evaluated at bearings #1 and #3. The results that are shown in Figure 22 and Figure 23 confirm that the theoretical vibrations obtained by applying the identified bending moments to the machine model are in good accordance with the respective experimental data.

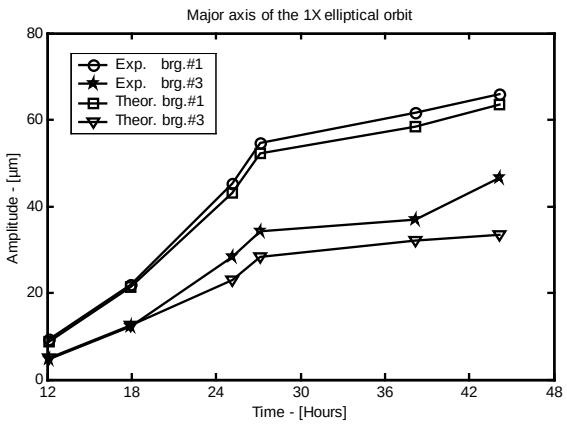

Figure 22: Comparison between experimental and theoretical amplitudes of the major axis of the 1X orbits described by the journal at bearings #1 and #3.

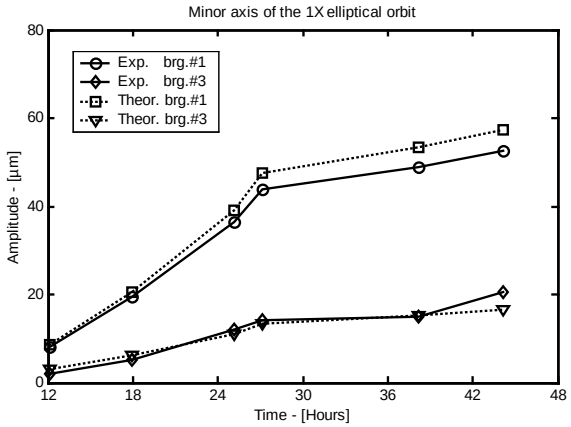

Figure 23: Comparison between experimental and theoretical amplitudes of the minor axis of the 1X orbits described by the journal at bearings #1 and #3.

The two pairs of equivalent 1X bending moments are applied at the same time in two fixed orthogonal planes as shown in eq. (15). These moments are vector quantities, therefore it is possible to evaluate the instantaneous resultant vector, M_1, during a complete rotation of the shaft. In general, the amplitudes of the two pairs of the opposite bending moments, $M_1^{(x)}$ and $M_1^{(y)}$, are not equal while the phase shift between $M_1^{(x)}$ and $M_1^{(y)}$ can differ from 90° degrees. Therefore, the resultant vector M_1 is not necessarily a rotating vector (1X) the amplitude of which is constant. The curve described by the end of this vector during a complete rotation of the shaft has been plotted in a polar plane (Figure 24).

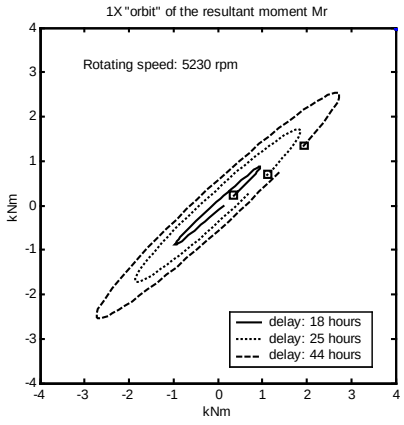

Figure 24: Orbits described by the end of the resultant vector M_1 of the identified bending moments.

The equivalent bending moments associated with three different stages of the crack propagation have been considered. The ellipses described by the end of the vector M_1 are rather flat. That is the degree of ellipticity is so high that these ellipses tend to degenerate into a straight line the inclination angle of which is 38°.

Further case studies carried out considering different sub–set of vibration data collected during the fault development showed similar results. This indicates that the equivalent excitations

associated with the crack breathing and the machine misalignment could be modelled with only one pair of 1X opposite bending moments applied in a fixed plane the inclination angle of which was nearly 38° with respect to the horizontal axis.
A further identification process of the fault was carried out by considering two pairs of opposite bending moments applied in the horizontal and vertical diametrical planes in the cross–section B, that is near the coupling flange towards the load gear shaft (Figure 9). The equivalent excitations were identified with the same approach above described. In this case the mean value and the standard deviation of the residuals obtained with the identification method were 1.4847 and 0.0103 respectively. These results indicate that when the fault location has been supposed to be near the coupling end towards the gearbox the identification errors were rather large. In fact, the experimental findings pointed out that the coupling yielding occurred in the weld area towards the gas turbine (cross–section A). This confirms the reliability of the results provided by the fault identification method.

4. CONCLUSION

Load couplings mounted in the shaft–train of rotating machines can be affected by the propagation of cracks. Abnormal machine misalignments due to incorrect maintenance actions as well as to large differences between hot dynamic alignment and cold static alignment make the crack propagation easier. Owing to the flexural flexibility of diaphragms and membrane units the shaft vibrations may not be affected by some typical symptoms (2X vibration changes) that allow shaft cracks to be timely detected. This may cause unexpected catastrophic failures.
This paper shows the main results obtained with a model–based analysis of the shaft vibrations caused by the propagation of a crack occurred in the load coupling connected to the gas–turbine of a power unit. Too high alarm levels of the machine vibrations, masked fault symptoms and the absence of a predictive monitoring strategy allowed a catastrophic failure to occur.
An original diagnostic strategy has been used to point out clear symptoms of the impending failure in the 1X instead of 2X vibrations by means of the analysis of the monitoring data. Moreover, the vibrations caused by the shaft bow due to the propagation of the crack have been simulated with suitable equivalent excitations the magnitude and phase of which have been estimated by means of a model–based identification method.
The successful results obtained with this investigation have confirmed the good capabilities of the diagnostic strategies that has been used. Their application in the case study described in the paper would have allowed the crack generated in the load coupling to be timely detected and the catastrophic failure to be avoided.

APPENDIX. - CRACK IDENTIFICATION METHOD

The identification of a crack, the dynamical effect of which is taken into account by means of a equivalent excitation system, is a special case of the general model based fault identification method presented in [7][8]. Only a summary is reported for clarity in this section.
It can be shown that the overall behaviour of a heavy horizontal cracked shaft is linear. Only in extreme operating conditions, the non-linear effect of the breathing crack, which is weak in normal conditions, may influence its behaviour.

Therefore, in a experimental case, the difference $\mathbf{x}_a = \mathbf{x}_{total} - \mathbf{x}_{ref.}$, between the measured vibration $\mathbf{x}_{total}$ of a rotor system that has a crack and the reference case $\mathbf{x}_{ref.}$ (previously stored in normal operating conditions), represents the vibrational behaviour due to the crack, which is defined as *additional vibrations.* These vibrations are used in the identification procedure, since they are due to the impending fault only. In fact, the reference case vibrations $\mathbf{x}_{ref.}$ are given by eq. (16):

$$[\mathbf{M}]\ddot{\mathbf{x}}_{ref.} + [\mathbf{C}]\dot{\mathbf{x}}_{ref.} + [\mathbf{K}]\mathbf{x}_{ref.} = \mathbf{F}_e \tag{16}$$

while those caused by the developing crack are given by:

$$[\mathbf{M}]\ddot{\mathbf{x}}_{total} + [\mathbf{C}]\dot{\mathbf{x}}_{total} + [\mathbf{K}_m]\mathbf{x}_{total} = \mathbf{F}_e + \widehat{\mathbf{F}}_{f_0} + \widehat{\mathbf{F}}_{f_1} e^{\,i\Omega t} + \widehat{\mathbf{F}}_{f_2} e^{\,i2\Omega t} + \widehat{\mathbf{F}}_{f_3} e^{\,i3\Omega t} \tag{17}$$

If eq. (17) is considered for an unknown crack, also $[\mathbf{K}_m]$ is unknown. Anyhow it can be approximated by $[\mathbf{K}]$ of the uncracked shaft, from which it differs only very little: the crack affects the stiffness of one element only. Therefore the additional vibrations are given by:

$$[\mathbf{M}]\ddot{\mathbf{x}}_a + [\mathbf{C}]\dot{\mathbf{x}}_a + [\mathbf{K}]\mathbf{x}_a = \widehat{\mathbf{F}}_{f_0} + \widehat{\mathbf{F}}_{f_1} e^{\,i\Omega t} + \widehat{\mathbf{F}}_{f_2} e^{\,i2\Omega t} + \widehat{\mathbf{F}}_{f_3} e^{\,i3\Omega t} \tag{18}$$

By applying the harmonic balance criteria in the frequency domain and considering the additional vibrations $\mathbf{X}_n$, the following equations are obtained for each harmonic component:

$$\left[-(n\Omega)^2\mathbf{M} + in\Omega\mathbf{C} + \mathbf{K}\right]\mathbf{X}_n = \mathbf{F}_{f_n} \quad n = 1,2,3 \tag{19}$$

in which the equivalent excitation vector $\mathbf{F}_{f_n}$, has to be identified. For simplicity, a single crack is considered. The extension to several cracks is very simple, by considering the sum of the equivalent $\mathbf{F}_{f_n}^{(k)}$, but this case is of scarce practical importance and rather improbable in real machines.

During a speed transient, for instance a coast-down, the condition monitoring systems of the machine collect data for many rotating speeds, so the additional vibrations are available for several rotating speeds and a set of n_p rotating speeds is considered:

$$\mathbf{\Omega} = \left\{\Omega_1 \quad \Omega_2 \quad \dots \quad \Omega_{n_p}\right\}^{\mathrm{T}} \tag{20}$$

Then, introducing the admittance matrix $\left[\mathbf{E}\left(n\mathbf{\Omega}\right)\right]$ of the system:

$$\left[\mathbf{E}(\mathbf{\Omega})\right] = \left[-(n\mathbf{\Omega})^2\mathbf{M} + in\mathbf{\Omega}\mathbf{C} + \mathbf{K}\right] \quad n = 1,2,3 \tag{21}$$

eq. (19) is expanded for all the considered rotating speeds of $\mathbf{\Omega}$:

$$\left[\mathbf{E}\left(n\boldsymbol{\Omega}\right)\right]\ \mathbf{X}_n = \begin{bmatrix} \mathbf{E}\left(n\Omega_1\right) & 0 & 0 & 0 \\ 0 & \mathbf{E}\left(n\Omega_2\right) & 0 & 0 \\ \vdots & \vdots & \vdots & \vdots \\ 0 & 0 & 0 & \mathbf{E}\left(n\Omega_{n_p}\right) \end{bmatrix} \begin{Bmatrix} \mathbf{X}_n \\ \mathbf{X}_n \\ \vdots \\ \mathbf{X}_n \end{Bmatrix} = \mathbf{F}_{f_n}, \quad n = 1,2,3 \tag{22}$$

The identification problem in eq. (22) is overdetermined since the number of the observation (the measured vibrations at different rotating speeds) are greater than the number of the parameters of the equivalent excitation that have to be identified.

Let the machine model have n_r nodes and n_b measuring planes in which the vibrations $\mathbf{X}_{\mathrm{B}mn}$ are measured at n_p rotating speeds generally in two orthogonal directions, and the supporting structure is represented by means of a foundation with n_f d.o.f.s. The d.o.f.s of the fully assembled model are $(4n_r + n_f)$ while only $2n_b$ d.o.f.s are measured per each rotating speed. Note that n_e, number of elements, is $n_r - 1$.

In general, since the equivalent excitation has to be identified not only in its magnitude but also in its position, the procedure has to be repeated per each node/element of the rotor, unless the research of the fault is limited to a specific position or to an interval of the nodes/elements.

Eq. (22) represents the general system of equations for all the d.o.f.s of the considered fully assembled machine. The admittance matrix $\left[\mathbf{E}(n\boldsymbol{\Omega})\right]$ has order $\left((4n_r + n_f)n_p \times (4n_r + n_f)n_p\right)$.

Now, least square identification is used here in order to evaluate the module, the phase and a residual of the equivalent excitation, starting from the first element and moving along the rotor from element to element. Weighted least square error method or more sophisticated techniques can be employed in order to increase the robustness of the identification as described in [7] and [20].

The equivalent excitation system, is applied in each element of the rotor model, so the fault vector is of order $\left((4n_r + n_f)n_p \times 2\right)$ for all the rotating speeds. Therefore, in the first element, the localization matrix for the *i*-th rotating speed is:

$$\left[\mathbf{F}_{L_1}\right]^{(i)} = \left[\begin{array}{cccc|cccc|c|ccc} 0 & i & 0 & 0 & 0 & -i & 0 & 0 & \vdots & 0 & 0 & & 0 \\ \underbrace{0 \quad 0 \quad 0 \quad 1}_{1^{\text{st}}\text{ rotor node}} & & & & \underbrace{0 \quad 0 \quad 0 \quad -1}_{2^{\text{nd}}\text{ rotor node}} & & & & & 0 & \underbrace{0 \quad \cdots \quad 0}_{\text{foundation d.o.f.s}} & & \end{array}\right]^{\mathrm{T}} \tag{23}$$

and for all the n_p rotating speeds:

$$\mathbf{F}_{L_1} = \begin{Bmatrix} \left[\mathbf{F}_{L_1}\right]^{(1)} \\ \vdots \\ \left[\mathbf{F}_{L_1}\right]^{(n_p)} \end{Bmatrix} \tag{24}$$

The effect on the measured d.o.f.s $\left[\hat{\mathbf{X}}_{\mathrm{B}_n}\right]$, which vector is of order $(2n_b n_p \times 1)$, due to unitary excitation systems applied to the selected element of the model is now calculated. This is done by first substituting eq. (23) in the right hand side of eq. (22), and inverting matrix $\left[\mathbf{E}(n\boldsymbol{\Omega})\right]$, obtaining the matrix $\left[\mathbf{H}(n\boldsymbol{\Omega})\right]$.

$$\mathbf{X}_n = \left[\mathbf{E}\left(n\boldsymbol{\Omega}\right)\right]^{-1}\mathbf{F}_{f_n}(\boldsymbol{\Omega}) = \left[\mathbf{H}\left(n\boldsymbol{\Omega}\right)\right]\mathbf{F}_{f_n}(\boldsymbol{\Omega}), \quad n = 1,2,3 \tag{25}$$

Then, the vibrations of the d.o.f.s, which are measured, are separated from the remaining d.o.f.s of the system, by considering only the rows of $\left[\mathbf{H}(n\boldsymbol{\Omega})\right]$ corresponding to the measured d.o.f.s. The partitioned matrix is of order $\left(2n_b n_p \times (4n_r + n_f)n_p\right)$ and following eq. (26) is obtained:

$$\left[\hat{\mathbf{X}}_{\mathrm{B}n}\right] = \left[\mathbf{H}\left(n\boldsymbol{\Omega}\right)\right]\Big|_{\substack{mesured \\ d.o.f.s}}\mathbf{F}_{L_1}, \quad n = 1,2,3 \tag{26}$$

Now the complex vector $\overline{\mathbf{A}}_n = \left\{\overline{A}_n^{(x)} \quad \overline{A}_n^{(y)}\right\}^{\mathrm{T}}$ (i.e. the module and the phase for each harmonic component and direction) of the equivalent excitation system, applied to the selected element, that fits best the experimental data $\mathbf{X}_{\mathrm{B}m_n}$, of order $\left(2n_b n_p \times 1\right)$, has to be estimated. The fitting is done in least square sense, since the number of the unknown (modules and phases) is less than the equations (recalling that data are corresponding to several rotating speeds and each of the sets is composed by several measuring planes). The problem is equivalent to:

$$\min\left\|\left[\hat{\mathbf{X}}_{\mathrm{B}_n}\right]\overline{\mathbf{A}}_n - \mathbf{X}_{\mathrm{B}m_n}\right\|, \quad n = 1,2,3 \tag{27}$$

the general solution of which is given by means of the pseudo-inverse calculation:

$$\overline{\mathbf{A}}_n^{(1)} = \begin{Bmatrix} M_n^{(x),(1)} e^{i\varphi_n^{(x),(1)}} \\ M_n^{(y),(1)} e^{i\varphi_n^{(y),(1)}} \end{Bmatrix} = \left(\left[\hat{\mathbf{X}}_{\mathrm{B}n}\right]^{\mathrm{T}}\left[\hat{\mathbf{X}}_{\mathrm{B}n}\right]\right)^{-1}\left[\hat{\mathbf{X}}_{\mathrm{B}n}\right]^{\mathrm{T}}\mathbf{X}_{\mathrm{B}mn}, \quad n = 1,2,3 \tag{28}$$

The module and the phase of the complex value in the rows of $\overline{\mathbf{A}}_n^{(1)}$ are the equivalent bending moments due to the crack, in the selected element. Finally the residual in the selected element is determined, by first obtaining the calculated response due to the identified fault in the selected element:

$$\mathbf{X}_{\mathrm{B}n} = \left[\hat{\mathbf{X}}_{\mathrm{B}n}\right]\overline{\mathbf{A}}_n^{(1)}, \quad n = 1,2,3 \tag{29}$$

and then by normalizing it:

$$\delta_{r_n}^{(1)} = \left(\frac{\left[\mathbf{X}_{\mathrm{B}_n} - \mathbf{X}_{\mathrm{B}m_n} \right]^{*\mathrm{T}} \left[\mathbf{X}_{\mathrm{B}_n} - \mathbf{X}_{\mathrm{B}m_n} \right]}{\mathbf{X}_{\mathrm{B}m_n}^{*\mathrm{T}} \mathbf{X}_{\mathrm{B}m_n}} \right)^{1/2}, \quad n = 1,2,3 \tag{30}$$

The procedure is then iterated for all the n_e elements of the rotor. If a fault only is considered, a set in $\mathbb{R}$ of relative residuals given by eq. (30), ordered by the element number, is obtained:

$$\boldsymbol{\delta}_{r_n} = \left(\delta_{r_n}^{(1)}, \ldots, \delta_{r_n}^{(n_r - 1)} \right), \quad n = 1,2,3 \tag{31}$$

A graph representing the values of $\boldsymbol{\delta}_{r_n}$ along the shaft axis (from the first to the last element) can be drawn. The location that corresponds to the minimum value of $\boldsymbol{\delta}_{r_n}$ indicates the most probable location of the crack, the estimated equivalent excitation of which is given by the corresponding values $\mathbf{M}_n = M_n^{(x)} e^{i\varphi_n^{(x)}} + M_n^{(y)} e^{i\varphi_n^{(y)}}$ of eq. (28). The closer to zero the minimum value of eq. (31) is, the better the estimation of the equivalent excitation is per each harmonic component.

REFERENCES

[1] Saavedra, P.N. and Ramírez, D.E., "Vibration analysis of rotors for the identification of shaft misalignment – Part 1: theoretical analysis", *IMechE Proceedings of the Institution of Mechanical Engineers Part C-Journal of Mechanical Engineering Science*, **218**(9), Sept. 2004, ISSN 0954-4062, pp. 971-985.

[2] Sekhar, A.S. and Prabhu, B.S., "Effects of Coupling Misalignment on Vibrations of Rotating Machinery", *Journal of Sound and Vibration*, **185**(4), 1995, pp. 655-671.

[3] Prabhakar, S., Sekhar, A.S. and Mohanty, A.R., "Vibration Analysis of a Misaligned Rotor-Coupling-Bearing system passing through the critical speed", *IMechE Proceedings of the Institution of Mechanical Engineers Part C-Journal of Mechanical Engineering Science*, **215**(12), Dec. 2001, pp. 1417-1428.

[4] Hu, W., Miah, H., Feng, N.S. and Hahn, E.J., "A Rig for Testing Lateral Misalignment Effects in a Flexible Rotor Supported on Three or More Hydrodynamic Journal Bearings", *Tribology International*, **33**(3-4), 2000, pp. 197-204.

[5] Tadeo, A.T. and Cavalca, K.L., "A comparison of flexible coupling models for updating in rotating machinery response", *J. Braz. Soc. Mech. Sci. & Eng.*, **25**(3), 2003, pp. 235-246.

[6] Bachschmid, N. and Pennacchi, P., "Model–based malfunction identification from bearing measurements", *Proc. IMechE 7th Int. Conference on Vibrations in Rotating Machinery*, Nottingham, UK, (2000). pp. 571–580.

[7] Pennacchi, P., Bachschmid, N., Vania, A., Zanetta, G.A. and Gregori, L., "Use of Modal Representation for the Supporting Structure in Model Based Fault Identification of Large Rotating Machinery: Part 1 – Theoretical Remarks", *Mechanical Systems and Signal Processing*, **20**(3), 2006, pp. 662-681.

[8] Bachschmid, N., Pennacchi, P.and Vania, A., "Identification of multiple faults in rotor systems", *Journal of Sound and Vibration*, **254**(2), 2002, pp. 327–366.

[9] Pennacchi, P. and Vania, A., "Diagnosis and model based identification of a coupling misalignment", *Shock and Vibration*, **12**(4), 2005, , pp. 293-308.

[10] Wowk, V., "Machine Vibration: Alignment", 2000, Mc Graw-Hill, New York.

[11] Muszyńska, A., "Rotordynamics", 2005, Taylor & Francis, Boca Raton, FL, pp. 771-778, 982.

[12] Rylatt, J.A. and Jur, T.A., "Analysis of cracking in the journal-to-hub connection of a large hollow roll", *Proceedings of the 1996 ASME International Mechanical Engineering Congress & Exhibition*, Nov 17-22 1996, Atlanta, GA, USA, pp. 1-6.

[13] Adams, M., "Rotating machinery vibration", 2001, Marcel Dekker Inc, Ney York, NY, p. 287.

[14] Wauer, J., "On the dynamics of cracked rotors: A literature survey", *Applied Mechanics Review*, **43**(1), 1990, pp. 13-18.

[15] Gasch, R., "A Survey of the Dynamic Behaviour of a Simple Rotating Shaft with a Transverse Crack", J*ournal of Sound and Vibration*, **160**(2), 1993, pp. 313-332.
[16] Dimarogonas, A.D., "Vibration of Cracked Structures. A State of the Art Review", *Engineering Fracture Mechanics*, **55**(5), 1996, pp. 831-857.
[17] Bachschmid, N., Pennacchi, P., Tanzi, E. and Vania, A., "Identification of Transverse Crack Position and Depth in Rotor Systems", *Meccanica*, **35**(6), 2000, pp. 563-582.
[18] Gounaris, G.D. and Papadopoulos, C.A., "Crack identification in rotating shafts by coupled response measurements", *Engineering Fracture Mechanics*, **69**(3), 2002, pp. 339-352.
[19] Pennacchi, P., Bachschmid, N. and Vania, A., "A model based identification method of transverse cracks in rotating shafts suitable for industrial machines", *Mechanical Systems and Signal Processing*, **20**(8), 2006, pp 2112-2147.
[20] Pennacchi, P., Vania, A. and Bachschmid, N., "Robust model based identification of faults in rotor dynamics using M-estimators", Paper-ID 96, *Proc. of IFToMM 7th International Conference on Rotor Dynamics*, Vienna, Austria, September 25-28, 2006, pp. 1-11.